Evaluating spatial patterns of drought-induced tree mortality in a coastal California pine forest

Citation	Baguskas, S. A., Peterson, S. H., Bookhagen, B., & Still, C. J. (2014). Evaluating spatial patterns of drought-induced tree mortality in a coastal California pine forest. Forest Ecology and Management, 315, 43-53. doi:10.1016/j.foreco.2013.12.020
DOI	10.1016/j.foreco.2013.12.020
Publisher	Elsevier
Version	Accepted Manuscript
Terms of Use	http://cdss.library.oregonstate.edu/sa-termsofuse

Evaluating spatial patterns of drought-induced tree mortality in a coastal California pine forest

Sara A. Baguskas[a,*], Seth H. Peterson[a], Bodo Bookhagen[a], Christopher J. Still[b]

[a] Department of Geography, University of California-Santa Barbara, Santa Barbara, California, 93106-4060, USA

[b] Forest Ecosystems and Society, Oregon State University, Corvallis, Oregon, 97331, USA

* Corresponding author: Tel.: 503-504-6854. *E-mail address:* baguskas@geog.ucsb.edu (S.A. Baguskas)

Abstract

In a coastal, fog-influenced forest on Santa Cruz Island in southern California, we observed mortality of Bishop pine (*Pinus muricata* D.Don) trees following a brief (2 year), yet intense, drought. While anecdotal evidence indicates that drought-induced Bishop pine mortality has occurred in the past in the stand we studied, this is the first attempt to capture the spatial distribution of mortality, and begin to understand the environmental drivers underlying these events. We used high spatial resolution remote sensing data to quantify the spatial extent of tree mortality using a 1 m true color aerial photograph and a 1 m lidar digital elevation model. We found the highest density of dead trees in the drier, more inland margins of the forest stand. We used the Random Forest decision tree algorithm to test which environmental variables (e.g., summertime cloud frequency, solar insolation, and geomorphic attributes) would best separate live and dead tree populations. We also included tree height as a variable in our analysis, which

we used as a proxy for overall tree size and potential rooting distribution. Based on the Random Forest analysis, we generated a map of the probability of survival. We found tree survivorship after drought was best explained by the frequency of summertime clouds, elevation, and tree height. Specifically, survivorship was greatest for larger trees (~8-10 m tall) in more foggy parts of the stand located at moderate elevation. We found that probability of survival was lowest at the inland extent of the stand where trees occur at the upper limit of their elevation range (~400 m). The coexistence of these main factors with other landscape variables help identify areas of suitable habitat for Bishop pines across the stand, and extend our understanding of this species' distribution.

Keywords: Tree mortality; Coastal fog; Drought-stress; Remote Sensing; Random Forest

1. Introduction

Across the western United States, widespread increases in tree mortality rates have been observed in recent decades (van Mantgem *et al.,* 2009). Many experimental, observational, and modeling studies attribute tree mortality to drought stress in response to regional warming (Anderegg, *et al.,* 2012; Allen *et al.,* 2010; Williams, *et al.,* 2010; Adams *et al.,* 2009; Breshears *et al.,* 2005; Allen and Breshears, 1998). To date, the geographical scope of studies of tree mortality in the American West has been limited to continental, montane climates (Hanson and Weltzin, 2000). Much less is known about the extent and frequency of drought-induced mortality events in coastal forests.

The maritime influence on weather and climate in coastal forests is assumed to buffer coastal ecosystems from extreme climate fluctuations, and therefore help maintain a stable

47 distribution of species over time. However, we observed extensive mortality of a coastal pine
48 species, Bishop pine (*Pinus muricata*, D.Don), following a brief, yet intense, drought period at
49 the southern extent of its range in California, where they are at the climatic margin that can
50 support the species (Williams *et al.*, 2008; Fischer *et al.*, 2009).

51 Throughout the Pliocene and Pleistocene, when the California climate was considered to
52 be more mesic compared to today, with year-round precipitation, Bishop pine, and closely
53 related Monterey pine (*P.radiata*), were more widely and evenly distributed along the California
54 coast (Raven and Axelrod, 1978). Bishop pine populations are currently restricted to a small
55 number of stands scattered along the fog-belt of coastal California and northern Baja California
56 (Lanner, 1999). The reduction of suitable habitat for Bishop pine (and similar coastal forests)
57 since the late Pleistocene is attributed to the onset of xeric Mediterranean climate conditions
58 (warmer temperatures, and reduced seasonal precipitation, occurring predominantly during the
59 winter). However, summer precipitation from fog drip, and potentially foliar uptake of fog water
60 (Limm *et al.*, 2009, 2010), is thought to enable Bishop Pines to persist along the coast and
61 offshore islands (Raven and Axelrod, 1978).

62 Fog water inputs to a forest, and its effects on the water relations of trees, are spatially
63 heterogeneous because deposition of fog water and shading effects of fog are controlled by a
64 variety of factors that range from the landscape to canopy scale. Fog is commonly defined as a
65 low-stratus cloud that intercepts land. The mechanisms by which fog ameliorates the water stress
66 of trees largely depend on their relative position to the fog layer. Shading effects, which reduce
67 evapotranspiration, will benefit trees that are below the fog layer (Fischer *et al.*, 2009). Plants
68 immersed in the fog layer benefit from direct water inputs because fog droplets deposit on leaves
69 and drip to the ground increasing shallow soil moisture (Carbone *et al.*, 2012; Fischer *et al.*,

2009; Corbin *et al.*, 2005; Dawson, 1998; Ingraham and Matthews, 1995; Harr, 1982; Azevedo and Morgan, 1974; Vogelmann, 1973). Moreover, vegetation type, and canopy structure of a forest, has been shown to strongly influence fog water deposition (Ponette-Gonzalez *et al.*, 2010; Hutley *et al.*, 1997). For instance, direct fog water inputs decrease from the windward edge of the forest to its interior (Weathers *et al.*, 1995), negatively impacting the water status of trees that receive less fog-water inputs in the interior (Ewing *et al.*, 2009). Such edge effects can also impact recruitment rate of trees, and ultimately forest structure (Barbosa *et al.*, 2010; del-Val *et al.*, 2006). In short, the effect of fog on the growth and persistence of tree species in fog-influenced ecosystems is strongly mediated by the spatial heterogeneity of the landscape, namely topographic variation and forest structure (Uehara and Kume, 2012; Gutierrez *et al.*, 2008; Cavelier *et al.*, 1996; Vogelmann, 1973). Since the influence of summer cloud shading and fog drip/immersion on the moisture regime of forested ecosystems vary spatially, it is reasonable to hypothesize that the risk of drought-induced mortality in a fog-influenced forest would follow suit.

The proportion of dead Bishop pines that followed the recent drought event increased from the coast inland, and mortality was more severe at the margins of the stand. These spatial patterns seemed to coincide with modeled water deficit, which included the influence of fog on the water budget of the ecosystem. Specifically, Fischer *et al.* (2009) found that the combined effects of fog drip and cloud shading can reduce summertime drought stress up to 56% in Bishop pine stands, and inland locations are particularly sensitive to reduced cloud shading and increased evapotranspiration compared to more coastal areas. While observations and water deficit models may infer that fog inundation and cloud shading are key climate variables explaining spatial patterns of tree mortality in this coastal forest, it is unlikely that a single

93 environmental variable, such as fog frequency, can entirely explain the spatial patterns of tree
94 mortality.

95 A suite of physical factors, such as landscape features (e.g., soil thickness and type, slope,
96 aspect, elevation, topography, and drainage networks), can generate stress gradients across the
97 landscape (Gitlin *et al*., 2006) and may explain the distribution of water stress in trees and tree
98 mortality just as well as spatial patterns of climate (Koepke *et al.,* 2010, Olge *et al.*, 2000). In
99 addition to landscape factors, biotic factors, such as tree size, may help predict mortality within a
100 forest stand (Floyd *et al.*, 2009). While trees at different life stages (for which size can be proxy)
101 may make different physiological adjustments to avoid or tolerate water stress, in general, it has
102 been argued that larger trees with an extensive rooting distribution should be more capable of
103 accessing stable water resources even during dry periods compared to smaller trees, and
104 therefore be less sensitive to drought conditions (Cavender-Bares and Bazzaz, 2000; Dawson,
105 1996; Donovan and Ehleringer, 1994). In particular, water status of larger, adult Bishop pines is
106 less affected by the summer dry period compared to smaller, sapling trees, which become water
107 stressed by late-summer (S. Baguskas, *unpublished data*). Understanding how interacting
108 environmental factors explain the spatial patterns of mortality will improve our ability to assess
109 the vulnerability of coastal forests to drought-induced mortality in the future.

110 Remote sensing is a powerful tool for quantifying the spatial extent of tree mortality,
111 which is often the first step towards elucidating patterns and processes underlying a mortality
112 event, such as drought stress (Allen *et al.,* 2010; Williams *et al.*, 2010; Macomber and
113 Woodcock, 1994), bark beetle infestation (Edburg *et al.,* 2012; Wulder *et al.*, 2006), and the
114 potential impacts on regional carbon budgets (Huang and Anderegg, 2012). While many studies
115 have quantified the spatial extent of tree mortality at regional and landscape scales using

116 moderate-spatial (>30-m ground resolution) resolution remote sensing data (e.g., Meigs *et al.,*
117 2011; Anderson *et al.*, 2010; Fraser and Latifovic, 2005), a growing number of studies have used
118 high-spatial (< 5-m ground resolution) resolution remote sensing data to examine tree mortality
119 at finer spatial scales in order to detect mortality of individual trees (or clusters) within a stand
120 (e.g., Stone *et al.*, 2012: Dennison *et al.*, 2010; Hicke and Logan, 2009; Chambers *et al.,* 2007;
121 Guo *et al.,* 2007; Coops *et al.,* 2006; Clark *et al.,* 2004). Developing a way to possibly make
122 large scale estimates and predictions of tree mortality based on remotely sensed data can help
123 land managers, who are tasked with making decisions about species and land conservation in the
124 future, respond to a future expected to become warmer and drier.
125 Our research addresses the following questions: 1) What is the spatial distribution of tree
126 mortality observed during the 2007-2009 drought period? 2) What is the correlative relationship
127 between environmental variables, such as climate, landscape features, and tree size, and the
128 spatial distribution of tree mortality? 3) Where is tree mortality likely to occur on the landscape
129 during periods of drought stress?
130
131 **3. Methods**
132 **3.1. Study Site**
133 This study was conducted in the westernmost and most extensive (3.6 km^2) Bishop pine
134 stand on Santa Cruz Island (SCI, 34^o N, 119^o 45' W), which is the largest of the northern islands
135 in Channel Islands National Park (~250 km^2 , 38 km E-W extension) located approximately 40
136 km south of Santa Barbara, CA (Figure 1). The Mediterranean climate along the California coast
137 and islands offshore is characterized by cool, rainy winters and warm, rain-free (yet foggy)
138 summers. While rainfall is highly variable both inter- and intra-annually, on average about 80%

of rain falls on SCI between December and March (Fischer *et al.*, 2009). We observed mortality of Bishop pines during water year 2006-07 and 2008-09, when fewer than 25 cm of rain fell (median rainfall is 43 cm) (Figure A1). In 2009, we observed peak mortality of Bishop pine trees in the field based on the high number of tree canopies with red foliage, and we found that no other plant species exhibited a mortality response like the Bishop pines did.

The Bishop pine stand that we studied exists on complex and rugged terrain ranging from sea level to just over 400 m in elevation. Bishop pines are almost entirely restricted to the wetter, cooler north-facing slopes. There are only a few scattered clusters of trees that exist on the drier south-facing slopes, and those tend to occur in drainages. Steep ridges rise from the Santa Cruz Island fault that runs E-W through the central part of the island. There is a stark ecological and geographical difference between the northern and southern sections of the island. The northern half of the island is composed of Santa Cruz Island volcanics and is sparsely vegetated compared to the southern half, which is mostly metamorphic in origin and supports most of the vegetation (Junak *et al*., 1995). The habitat for woody vegetation is considered to be more suitable at the center of the largest Bishop pine stand where the canopies are continuous relative to the margins of the stand where pines are intermixed with more drought-tolerant coastal chaparral angiosperm plant species, such as Manzanita (*Arctostaphylos insularis, A. tomentosa*), Ceanothus (*Ceanothus arboreus, C.megacarpus subsp. insularis*), and Scrub Oak (*Quercus pacifica, Q. dumosa*).

3.2. Datasets

We used a variety of data sources to quantify the spatial variability and extent of tree mortality across the Bishop pine stand (Table A1). We included in our analysis Digital Orthophoto Quarter Quads (DOQQ), which are true color aerial photographs at 1-m spatial resolution, collected by the United States Geological Survey, from 2005 (pre-drought) and 2009

(post-drought). In order for us to accurately identify dead and live trees on a pixel-by-pixel basis, source images first needed to be georeferenced (i.e., aligned), with one another. The 2005 DOQQ was georeferenced to the 2009 DOQQ using 90 ground control points (GCPs) with root mean square error (RMSE) of 1.25 m. GCPs were selected from temporally invariant targets, such as road intersections. In conjunction with the DOQQ images, we used spectral information of different land cover types from an Airborne Visible Infrared Imaging Spectrometer (AVIRIS, 224 bands, 2.3 m) image collected by the Jet Propulsion Lab prior to the mortality event (7 August 2007). For the AVIRIS image, a geometric look-up table was applied to remove some of the geometric distortion for approximate georeferencing. We further improved the registration by georeferencing the AVIRIS image to the 2009 DOQQ using unambiguous reference points, such as road edges and distinct plant canopies (105 GCPs, 1.07 m RMSE).

Environmental variables used to explain the spatial patterns of tree mortality were derived from remotely sensed data (Table 1). These layers were already georeferenced. To evaluate the strength of the relationship between summertime cloud shading/fog immersion and tree mortality, we compared mortality to average summertime cloudcover frequency (Figure 2a). Average summertime cloudcover frequency was calculated from composite MODIS (Moderate Resolution Imaging Spectroradiometer) images at 250 m collected daily at 10:30 am PST from July to September between 2000 to 2006 (Williams, 2009; Fischer *et al.*, 2009). The 10:30 am PST overpass time of the Terra satellite captures the lingering fog from a heavy nighttime event, as the fog layer is often present until noon on SCI (Fischer *et al*., 2009; Carbone *et al.*, 2012). For each MODIS pixel, a quality control classification was assigned for one of three conditions: clear sky, partial cloud cover, or total cloud cover. We determined the average fraction of days each month (i.e., frequency) when the pixels covering our study sites were classified as partially

186 or totally cloudy using these quality classifications (Williams, 2009). In the summer, low-level
187 marine stratus clouds are the most common cloud types on the California coast (Iacobellis and
188 Cayan, 2013). Cloud frequency should be closely related to fog frequency, though information
189 on elevation is required to determine whether the clouds were overhead (shading effect) or at the
190 ground (i.e., fog immersion).

191 Four topographic layers (elevation, solar radiation, slope, and aspect) were included as
192 explanatory variables. These variables exert control on the water budget of an ecosystem, such as
193 the amount of solar radiation received by a surface (Dubayah, 1994). Topographic variables were
194 derived from a digital elevation model (DEM) generated from a dense Light Detection and
195 Ranging (LiDAR) point cloud collected by the USGS in January 2012. LiDAR return signals
196 were classified into bare-earth and vegetation points and we created a regularly spaced grid at 1
197 m spatial resolution. The resulting DEM (Figure 2b) has been verified in the field and found to
198 be very robust (cf. Perroy et al., 2010; Perroy et al., 2012). Field-based validation points were
199 similar in 2010 and 2012, though the density of return signals was greater in 2010. From the
200 DEM, we calculated average daytime solar radiation at the surface (i.e., insolation) for the
201 summertime months (1 June – 30 September) at 14-day intervals using standard GIS techniques
202 (Hetrick, *et al.,* 1993) (Figure 2c). The primary spatial variations in modeled cloud-free solar
203 insolation for these calculations are driven by slope, aspect, and elevation. Slope and aspect
204 (Figure 2e and 3f, respectively) were calculated from the DEM using standard algorithms.
205 Aspect was rotated by 180 degrees to avoid discontinuity on north-facing slopes, where Bishop
206 pines are most common (i.e. aspects of 1 degree and 359 degrees are not different ecologically
207 but are very different numerically). Therefore, north-facing slopes are 180 degrees, south-facing
208 slopes are 360 degrees, west-facing slopes are 90 degrees, and east-facing slopes are 270

209 degrees. We used the average value for solar insolation, elevation, slope, and aspect within a 3-m
210 radius from each tree point.

211 Attributes measuring the surface shape (i.e., the geomorphology of the landscape) can
212 help characterize how topography controls and integrates hydrologic processes on a range of
213 timescales (Monger and Bestelmeyer, 2006; Sorensen *et al.*, 2006; Moore *et al.*, 1991), and
214 therefore strongly influences the spatial distribution of soil moisture and groundwater. We
215 included a topographic wetness index (TWI), which describes the amount of water that
216 potentially accumulates in every given pixel (Moore *et al.*, 1991) (Figure 2g). This index was
217 calculated as (ln(upslope catchment area/slope)). We calculated the maximum values within a
218 4.5 m radius of each tree point to best represent the potential water accumulated at the rooting
219 zone of the tree, which we estimated to expand at least 1 -2 meters beyond the tree canopy. We
220 also included an estimate of the curvature (concavity and convexity) of the landscape, which
221 affects the flow path of water (Gessler *et al.*, 2000; Ali *et al*., 2010) (Figure 2h). Curvature is the
222 second derivative of the DEM. We calculated the average value of curvature within a 3 m radius
223 of each tree point.

224 Lastly, we included a data layer of vegetation height, which we calculated from the
225 classified lidar point cloud by analyzing the bare earth DEM and canopy-height DEM (Figure
226 2d). Because the point of live and dead trees identified in the DOQQ may not necessarily capture
227 the apex of the canopy in the lidar DEM, we calculated the maximum height for vegetation
228 within the 3-m radius of each tree point to more accurately represent the height of each tree.
229

230 **3.3. Map of tree mortality**

We identified dead trees manually in the 2009 DOQQ as areas of red pixels within the Bishop pine stand (Figure 3a). By combining this base image with the 2005 DOQQ (pre-drought), we were able to identify trees that died due to the drought period by identifying trees with red canopies in 2009 and green canopies in 2005 (Figure 3b). We validated our remotely sensed map of mortality by measuring distances between dead tree canopies in the field and corresponding nearest dead tree canopies identified in the map. We collected location data of dead (n=80) trees in the field using a differential GPS unit (Trimble Geoexplorer 6000 rover) in July 2010 with accuracy of < 15 cm. We aimed to sample areas with low and high density of tree mortality.

3.4 Random Forest analysis

We used the Random Forest (RF) decision tree algorithm (Breiman, 2001) implemented in R (R Development Core Team 2010 version 2.12.2) to identify environmental variables that best explain the distribution of dead trees, relative to live trees, across the Bishop pine stand. The RF sample population was composed of 1740 trees, of which 869 were identified as live, and 871 as dead, *a priori*. For each of these live and dead tree points, we extracted values from the environmental variable raster datasets (Table 1), and these values were used as input to the RF analysis.

Decision trees and RF are used to uncover complex hierarchical relationships between response variables and diverse environmental variables in multivariate data sets (Michelson *et al.,* 1994; Moore *et al.,* 1991). Non-linear and non-additive relationships are learned from the data rather than explicitly modeling them (Michaelsen et al. 1994, Bi and Chung 2011). Further, they are non-parametric models, which means that variable normality and independence

assumptions need not be met (Michaelsen et al. 1994, Bi and Chung 2011). Decision trees use threshold values of predictor variables to separate the response variable into more and more homogeneous groups, in our case live and dead tree populations. The RF approach aggregates the results from hundreds of individual decision trees to provide more robust predictions. Specifically, different decision trees are generated for the same data set by 1) using a sub-sample of the predictor variables at any given node (or split, based on threshold value) in the tree, and 2) using sub-samples of the response variable for training and testing each decision tree. Furthermore, values of each predictor variable are varied by +/- 10 percent and the resulting effect on classification accuracy is used to quantify variable importance through the Mean Decrease in Accuracy (MDA) score (range of 0 to 1) (Breiman, 2001). The greater the MDA score, the more important the variable is in separating live and dead tree populations. While the RF analysis ranks the importance of variables, it does not indicate the nature of the relationships between explanatory variables and the dependent variable. In order to identify and illustrate the nature of these relationships, we compared the histograms of live and dead tree populations for each of these variables, and conducted a Mann-Whitney U test (R version 2.12.2) to test for significant differences between median values at the $p<0.01$ level.

We acknowledge that some of the environmental variables used in our analysis are interdependent, e.g., slope correlates positively with solar insolation and elevation is correlated with cloudiness (Table A2). However, the use of correlated variables in RF analyses biases neither the classification output (because RF is non-parametric) nor the measure of variable importance (Bi and Chung 2011; Peterson *et al.*, 2012).

3.5. Predictive map of tree mortality

We created a predictive map of tree mortality using the RF results and the maps of environmental variables. Specifically, we used the R function 'yaimpute' (R version 2.12.2), which takes the 500 decision trees generated by the RF and applies them to the environmental variables. The algorithm then averages the 500 resulting predictor maps to make one final map. Areas where trees are more likely to die following drought are indicated by values closer to one, whereas trees in areas closer to zero are more likely to live. To better understand what environmental conditions characterize areas of low and high mortality during drought, we compared and contrasted average values of environmental variables at five sites that fall along a coastal inland elevation gradient established by Fischer *et al.* (2007). We examined mortality risk at these sites for two reasons: 1) sites varied in their levels of probability of mortality, and 2) field data on fog-water inputs were available for these locations providing an opportunity for us to relate our remotely sensed data of environmental factors with field observations related to potential moisture availability.

4. Results

4.1. Spatial pattern of tree mortality

We were able to accurately identify mortality of nearly 900 Bishop pine trees at 1-m spatial resolution (Figure 3b and 3c). To more clearly represent the spatial distribution of dead tree clusters across the stand, we generated a map of dead tree density (Figure 3d). While there are many isolated patches of dead trees in various locations within the stand, we found the highest density of dead trees to be in the eastern, more inland margin. We assessed the accuracy of our remote sensing approach with field validation points, and found that 30% of the remotely sensed dead trees were within 10 m of the ground points (n=80), and 33% of the dead trees were

between 10 and 20 m (Figure A2). In addition, visual inspection of the proximity of remotely sensed dead trees to field-based points revealed good agreement between the two datasets.

4.2. Relationship between environmental variables and tree mortality

The variables included in our RF analysis formed interacting, hierarchical relationships to distinguish dead (n=871) from live (n=869) tree populations within the stand. These variables, however, had different levels of importance (Table 3). Cloud frequency and elevation received a high rank by the RF analysis (Table 3, MDA: clouds = 0.84, elevation = 0.79), which suggests that the position of trees relative to the summertime stratus cloud layer is important for reducing the likelihood of mortality. Bishop pines on SCI grow along an elevation gradient that increases from the coast inland, and along this gradient, summertime cloud cover frequency decreases (Figure A3a). We found most of the dead trees were clustered at the upper limits of the elevation range within the stand (~360-400 m), where cloud frequency was lowest (Figure A3b), coinciding with where we observed the greatest tree mortality. Live trees spanned a broader range of elevation and cloud frequencies (Figure A3c). In particular, most Bishop pines that died were located at or above 350 m elevation (Figure 4a, median = 351 m) and where cloud frequency was less than 27% (Figure 4b, median = 0.26) compared to live trees that were more frequently found below 300 m (Figure 4a, median = 279 m) in cloudier parts of the stand (Figure 4b, median = 0.30).

Vegetation height was found to be of roughly equal importance to cloud cover and elevation in separating live and dead trees (Table 3, MDA: veg. height = 0.81). Dead trees were significantly shorter than live trees (Figure 4c; median dead = 7.4 m, median live = 9.0 m, $p<0.001$). We did not find a correlation between tree height and any of the environmental factors

used in our analysis; however, the spatial distribution of vegetation height indicates that taller trees dominate ridges in the southwest portion of the stand where tree mortality was minimal (Figure 2d).

The remaining topographic variables (solar insolation, slope, and aspect) contributed to distinguishing live and dead tree populations, yet were ranked lower than cloud frequency, elevation, and vegetation height (Table 3). Nonetheless, the degree of spread and skewness in the histograms revealed subtle, but interesting differences between groups. The absolute difference in median solar insolation values between live and dead tree populations was negligible; however, live trees were normally distributed over the entire range of solar insolation values, whereas dead trees occurred more often in areas of higher solar insolation (Figure 4d; median dead =19.5 MJ m^{-2}, median live = 18.5 MJ m^{-2}, $p<0.001$). Additionally, dead trees were found on more shallow slopes compared to live trees (Figure 4e; median dead = 25^{o}, median live = 30^{o}). Most Bishop pines (dead or live) grew on northeast-facing slopes, yet live trees were slightly more restricted to north-facing slopes compared to dead trees (Figure 4f; median dead= 194 degrees, live = 203 degrees).

Geomorphic variables that characterize the hydrologic environment (TWI and curvature) received the lowest MDA rank relative to other variables in the RF analysis (Table 3). Both live and dead trees tended to grow in partially channelized areas of the landscape as indicated by larger, positive values of TWI (Figure 4g). The negative curvature values for most of the trees indicate that they also grow in areas with convergent flow lines (Figure 4h). Certainly Bishop pines grow on ridges as well, but these results suggest growing in drainages where more water accumulates is important for tree growth, especially during dry years.

Of the three environmental variables with the highest importance (clouds, elevation, and vegetation height), clouds and vegetation height showed linear relationships with probability of mortality (correlations of 0.54 and 0.48 respectively). Elevation was not linearly correlated with mortality, though the high importance value of elevation suggests a non-linear or hierarchical relationship.

4.3. Accuracy Assessment for Random Forest analysis

An accuracy assessment of the RF analysis allows us to evaluate how well the RF algorithm classified live and dead trees based on the reference map we generated from the DOQQ. The accuracy of RF analysis is evaluated using a confusion matrix from which the Producer's, User's, and overall accuracy are derived (Table 2). Producer's accuracy refers to the probability that a certain land-cover category, e.g., dead trees, in the reference map was classified as such by the RF algorithm (Congalton, 1991). For example, the Producer's accuracy of dead trees was 77% because 674 pixels were modeled as 'dead' by the RF algorithm out of the total 871 identified as dead in our reference map. On the other hand, the User's accuracy refers to the probability that a pixel modeled as 'dead' is accurately modeled as dead by the RF algorithm (Congalton, 1991). For example, the User's accuracy for dead trees is 78% because 674 pixels were correctly modeled as dead out of the 863 total pixels modeled as such by the RF algorithm. The Producer's and User's accuracy results for live trees were similar to that of dead trees. Overall, the classification accuracy was high with a score of 78% (kappa 0.55). The kappa statistic incorporates misclassification information, so is a more robust measure of accuracy than overall classification accuracy (Congalton, 1991).

4.4. Predictive map of tree mortality

The predictive map identifies where trees were most vulnerable to drought-induced mortality across the Bishop pine stand given the RF results (Fig. 8). We present these results in terms of probability of mortality, where values closer to one indicate a greater probability of dying through a drought period. We found that the probability of mortality in the Bishop pine stand ranged from 30-75% and that trees growing in eastern and western margins of the stand were at greater risk of mortality (shades of red/brown) compared to the central and southwest portions of the stand (shades of blue) (Fig. 8).

We compared the probability of mortality and environmental conditions at five sites that fell along a coastal-to-inland elevation gradient for which we also had fog-water input data collected in the field (Fischer *et al.*, 2007) (Table 3). The sites represent the mid-to-high values of the mortality probability scale (54-70%), and for each area we present the average values of the environmental predictor variables (Table 3). Sites were generally characterized by steep (30-34°), north-facing slopes with moderate solar insolation (17.6-18.9 MJ m^{-2}). Sites tended to be located in drainages (~ -0.02 – 0.13 m m^{-2}) and where water accumulates (TWI, 7.9-9.1). There was greater variability in other environmental predictive variables across sites.

Site 1 is located at the western margin of the forest stand relatively close to the coast. Mortality risk is highest at this site (Table 3; probability of mortality = 70%). Of the five sites, site 1 has the highest cloud frequency (32 %), yet the lowest average fog water input over the summer (597 ml). This is likely attributed to its position below the cloud layer (elevation 141 m). Trees are shorter (5.4 m tall) than at most other sites. Site 2 is slightly higher in elevation (201 m). While less cloudy (28%) than site 1, it receives more fog-drip (938 ml) (Table 3). Trees are relatively tall (9.7 m) here and mortality risk low (56 %). Site 3 is at higher elevation (423 m),

391 with the highest solar insolation (18.9 MJ m^{-2}) of all the sites. This site has moderate values of
392 cloud cover frequency (26%), fog-drip (1300 ml), vegetation height (7.8 m), and risk of mortality
393 (63%) relative to other sites. Site 4 is located at the far eastern margin of the Bishop pine stand,
394 close in elevation to site 3 (390 m). Probability of mortality (64 %) is also similar to that at site 3.
395 While cloud frequency is low (24 %), fog-drip (~1900 ml) exceeded that collected at most other
396 sites. Like site 1, vegetation was relatively short (6 m). Site 5 is located in the southwest portion
397 of the stand at moderate elevation (275 m) where cloud frequency is high (31 %) and receives
398 the most fog-drip (3205 ml). Trees are tall (11 m) and grow on northwest facing slopes (131°).
399
400 **5. Discussion**
401 *Spatial patterns of tree mortality*
402 We accurately identified approximately 900 dead Bishop pine tree clusters in the largest
403 Bishop pine stand on SCI. While we are confident that the high-spatial resolution of the 2009
404 DOQQ captured larger trees with red canopies when the photo was acquired (Figure 3b), we
405 believe that we under-sampled smaller trees (saplings) that we know died during the 2007-2009
406 drought period, based on field observations. For example, the DOQQ could not have captured
407 smaller trees growing beneath the canopy of larger trees (Meentemeyer *et al.*, 2008), or simply
408 canopies too small to be detected at 1-m spatial resolution, e.g., sub-meter diameter or seedlings.
409 Furthermore, we observe that there were smaller trees that died, or were very close to dead tree
410 canopies, based on the vegetation height data derived from the LiDAR dataset (Figure 4c), which
411 has much higher precision compared to an aerial photo.
412 The discrepancy between field-validation points and the remotely sensed trees (Figure A2)
413 was likely attributed to the temporal disconnect between when we identified dead trees remotely

(June 2009) and when we collected validation points (July 2010). Because many dead trees that expressed red needles in 2009 had lost their needles by July 2010, we could not identify in the field exactly which trees we identified in our remotely sensed map of mortality. Despite these shortcomings, the techniques used to identify dead trees were robust, and feel that we captured the majority of the trees that died in response to drought.

Environmental controls on tree mortality

Our study demonstrates that there is an inverse relationship between drought-induced mortality of Bishop pines and the occurrence of summertime clouds along a coastal inland elevation gradient on SCI. The spatial clustering of dead trees in the eastern, and more inland, margin of the stand is consistent with predictions from previous research. Fischer *et al.* (2009) characterized this area as marginal habitat for Bishop pine based on higher modeled soil water deficit, which incorporated the cloud frequency variables used in our analysis, as well as fog water volumes collected from the field. The occurrence of fog is spatially heterogeneous, thus the strength of its impact on reducing water stress and supporting tree growth depends on how it interacts with other landscape and forest elements, such as canopy height.

The vegetation height dataset derived from the 1-m LiDAR DEM provided us with a unique opportunity to address how characteristics of vegetation interact with climatic and landscape variables. We found that larger trees (>8 m tall) that occurred in cloudier, and thus foggier, areas (~30% summertime cloud frequency, Figure 2a and 3d) had high survivorship following drought. This agrees with previous research that showed Bishop pines had higher summertime growth rates in the cloudier portion of the stand compared to trees that grow further inland and at higher elevation (Carbone *et al*, 2012). The positive relationship between fog

frequency, tree size, and survivability could be explained by the fact that larger trees having a greater capacity to intercept fog and generate fog drip to the soil, which can significantly offset the effects of drought stress and support growth even during low rainfall years (Fischer *et al.* 2009; Carbone *et al.*, 2012). Therefore, fogginess may confer a fitness advantage over trees that grow in the less foggy, and more xeric parts of the stand (del-Val *et al.*¸2006), which has important implications for the local distribution of trees that persist at the water-limited extent of the species range.

Environmental heterogeneity and probability of mortality

The occurrence of low-stratus clouds in the summertime is not the only factor important to the survival of Bishop pine trees during drought. Complex and subtle interactions between climate, topography, and vegetation can have large effects on plant-available water, and the suitability of habitat for growth and survival. We observed that the three main distinguishing factors between sites with the highest and lowest mortality risk (Table 3; site 1 and site 5, respectively) were elevation, volume of fog-drip, and vegetation height (Table 3). Because cloudiness was equally high at both sites (~31-32%), the large difference in fog water input is attributed to where the low-stratus clouds are intercepted by land. Based on a climatology of cloud base heights from the Santa Barbara airport, interception of low-stratus clouds is 40% more likely at sites between 240-280 m than at lower elevation (B. Rastogi, pers. comm). Therefore, topographic relief is necessary for cloudiness to translate to direct fog water inputs, which influences plant-available water (Fischer *et al.*, 2007). In addition, trees were twice as tall at site 5 than site 1 (Table 3).

459 The probability of mortality was similarly low between sites 2 and 5. While these sites
460 supported the tallest trees, they were dissimilar with respect to other environmental variables.
461 Unlike site 5, site 2 is located at the mouth of a large drainage in the central valley on SCI, which
462 supports cool, wet conditions compared to sites located in more exposed areas. Because ridges
463 rise steeply from the valley floor, this site is also located on a steep, north-facing slope, which
464 explains why solar insolation was low compared to other sites (Table 3).
465 The similarity in probability of mortality at sites 3 and 4 (63 and 64 %, respectively)
466 coincide with many of the environmental factors that characterize these sites. Located on ridges
467 at the upper limit of the elevation range for Bishop pines on the island (~ 400 m) where cloud
468 frequency was relatively low (24-26 %) suggests that the evaporative losses may dominate at
469 these sites. The distinguishing factor between these sites, other than measured fog-drip, is
470 vegetation height. Trees are taller at site 3, therefore may have greater access to groundwater,
471 which could compensate for lower fog-water inputs. Conversely, trees at site 4 are shorter, but
472 grow on steeper slopes and are less exposed, thus buffered from drying effects.
473 The results of our study indicate that microhabitat conditions in the Bishop pine stand on
474 SCI are critical for determining the survival and persistence of trees during exceptionally warm,
475 dry periods. However, just as environmental conditions can vary widely across a forested
476 ecosystem, many studies have demonstrated that variation in physiological adjustments of trees
477 to stressful conditions, and differential growth patterns, are strong predictors of spatial patterns
478 of mortality in forests (McDowell *et al.*, 2008; Suarez *et al.*, 2004; Wycoff and Clark, 2002;
479 Olge *et al*., 2000; Pederson, 1998; Cregg, 1994). While we did not explicitly test for variation in
480 physiological responses or growth of Bishop pine trees in response to drought, we did find
481 mortality risk varied among trees of different size classes. The probability of mortality was

greater for shorter trees, even if the height difference was only 1-2 m (Figure 4d). One possible explanation for this pattern could be that smaller trees have limited access to stable water reserves deeper in the soil, thus are at a disadvantage during drought periods compared to larger trees that have a greater root:shoot ratio (Suarez *et al.*, 2004). Another interpretation of this pattern may be related to how drought has historically affected population dynamics (i.e., tree age and size structure) in the Bishop pine stand.

The most recent drought period (2007-09) was not an isolated event. Periodic droughts have affected the local distribution of Bishop pine on SCI in the past (Walter and Taha, 2000). The last major drought occurred between years 1986 and 1991, and killed off large swaths of Bishop pines across the island, particularly at the margins of the Bishop pine stands (Walter and Taha, 2000; Lyndal Laughrin, *pers. comm.*). Our results support the idea that survivorship of Bishop pine trees is compromised at the stand margins during drought (Figure 3). However, regeneration of the pine population in these areas has not ceased (Fischer *et al.*, 2009). The net effect of these drought cycles are even-aged cohorts dominating the stand margins. Therefore, the majority of trees we observed die after the most recent drought likely emerged following the previous drought that ended in 1991; thus, they were younger and had a shorter stature than the trees more resilient to drought stress that dominate the central and southwest parts of the stand.

Implications for management

Analyzing high-spatial resolution (1 m) aerial imagery and LiDAR remotely sensed data of tree mortality can provide more precise spatial information about the growing conditions of individual trees, or small tree clusters, and provide a more efficient approach to forest inventory (Maggi and Meentemeyer, 2002; Hicke *et al.,* 2012). Specifically, the color infrared DOQQ used

505 in our study clearly showed red-attack trees allowing us to delineate dead tree canopies. DOQQ
506 imagery is available at no cost and collected 2-3 times per decade for any given local in the
507 United States; therefore, acquiring and analyzing imagery that bookends a mortality event is
508 feasible, allowing for a cost-effective method of inventorying forest damage. In contrast, LiDAR
509 data is expensive and not readily available but the utility of deriving vegetation height and
510 landscape variables was clearly demonstrated in this project.

511 We found RF to be a power statistical tool for analyzing a large multivariate dataset that
512 ranked a suite of environmental variables used to predict tree mortality. This approach can be
513 used in a variety of forest management applications that require analysis of large datasets where
514 there may be correlation among the predictors and hierarchical and/or non-linear relationships
515 between predictor and response variables.

516 This study supports the idea that low-stratus summertime clouds are important to survival
517 of Bishop pines during drought periods at the most southern and water-limited extent of its
518 range. However, the distribution of this species is restricted to the narrow fog-belt of California,
519 despite the fact that precipitation is much higher further north, so fog must play a role in the
520 more northern parts of the range as well. There is a great amount of uncertainty surrounding how
521 the spatial and temporal variability of fog may change in the future; however, evidence suggests
522 that fog frequency may decline in parts of the California coastline (Johnstone and Dawson,
523 2010), which would have negative effects on the distribution of Bishop pines and other fog-
524 dependent species.

525

526

Acknowledgements: This work was funded by a grant from Kearney Foundation of Soil Science. We would like to thank Carla D'Antonio, Jennifer King, and Doug Fischer for helpful comments and valuable suggestions; Ryan Perroy for assistance in the field; The Nature Conservancy and the University of California Natural Reserve System for access to southwestern Santa Cruz Island.

Literature Cited

Adams, H.D., Guardiola-Claramonte, M., Barron-Gafford, G. A., Villegas, J.C., Breshears, D.D., Zou, C.B., Troch, P. A, Huxman, T.E., 2009. Temperature sensitivity of drought-induced tree mortality portends increased regional die-off under global-change-type drought. Proceedings of the National Academy of Sciences 106, 7063–6.

Ali, G. A., Roy, A.G., 2010. Shopping for hydrologically representative connectivity metrics in a humid temperate forested catchment. Water Resources Research 46, W12544.

Allen, C.D., Breshears, D.D., 1998. Drought-induced shift of a forest-woodland ecotone: rapid landscape response to climate variation. Proceedings of the National Academy of Sciences 95, 14839–42.

Allen, C.D., Macalady, A.K., Chenchouni, H., Bachelet, D., McDowell, N., Vennetier, M., Kitzberger, T., Rigling, A., Breshears, D.D., Hogg, E.H. (Ted), Gonzalez, P., Fensham, R., Zhang, Z., Castro, J., Demidova, N., Lim, J.H., Allard, G., Running, S.W., Semerei, A., Cobb, N., 2010. A global overview of drought and heat-induced tree mortality reveals emerging climate change risks for forests. Forest Ecology and Management 259, 660–684.

Anderegg, W.R.L., Berry, J. A, Smith, D.D., Sperry, J.S., Anderegg, L.D.L., Field, C.B., 2012. The roles of hydraulic and carbon stress in a widespread climate-induced forest die-off. Proceedings of the National Academy of Sciences 109, 233–7.

Anderson, L. O., Malhi, Y., Aragão, L. E., Ladle, R., Arai, E., Barbier, N., Phillips, O., 2010. Remote sensing detection of droughts in Amazonian forest canopies. New Phytologist, 187, 733-750.

Azevedo, J., Morgan, D.L., 1974. Fog precipitation in coastal California forests. Ecology, 1135-1141.

557 Barbosa, O., Marquet, P. A., Bacigalupe, L. D., Christie, D. A., Del-Val, E., Gutierrez, A. G.,
558 Jones, C.G., Weathers, K.C., Armesto, J. J., 2010. Interactions among patch area, forest
559 structure and water fluxes in a fog-inundated forest ecosystem in semi-arid Chile.
560 Functional Ecology 24, 909-917.

561 Bi, J., Chung, J., 2011. Identification of drivers of overall liking–determination of relative
562 importances of regressor variables. Journal of Sensory Studies 26, 245-254.
563
564 Breiman, L., 2001. Random forests. Machine learning 45, 5-32.

565 Breshears, D.D., Cobb, N.S., Rich, P.M., Price, K.P., Allen, C.D., Balice, R.G., Romme, W.H.,
566 Kastens, J.H., Floyd, M.L., Belnap, J., Anderson, J.J., Myers, O.B., Meyer, C.W., 2005.
567 Regional vegetation die-off in response to global-change-type drought. Proceedings of the
568 National Academy of Sciences 102, 15144–8.

569 Carbone, M.S., Williams, A.P., Ambrose, A.R., Boot, C.M., Bradley, E.S., Dawson, T.E.,
570 Schaeffer, S.M., Schimel, J.P., Still, C.J., 2012. Cloud shading and fog drip influence the
571 metabolism of a coastal pine ecosystem. Global Change Biology 19, 484-497.

572 Cavender-Bares, J., Bazzaz, F.A., 2000. Changes in drought response strategies with ontogeny in
573 *Quercus rubra*: implications for scaling from seedings to mature trees. Oecologia 124, 8-18.

574 Cavelier, J., Solis, D., Jaramillo, M. A., 1996. Fog interception in montane forests across the
575 Central Cordillera of Panama. Journal of Tropical Ecology 12, 357-369.

576 Chambers, J.Q., Asner, G.P., Morton, D.C., Anderson, L.O., Saatchi, S.S., Espírito-Santo,
577 F.D.B., Palace, M., Souza, C., 2007. Regional ecosystem structure and function: ecological
578 insights from remote sensing of tropical forests. Trends in Ecology & Evolution 22, 414–23.

579 Clark, D.B., Castro, C.S., Alvarado, L.D.A., Read, J.M., 2004. Quantifying mortality of tropical
580 rain forest trees using high-spatial-resolution satellite data. Ecology Letters 52–59.

581 Congalton, R.G., 1991. A Review of Assessing the Accuracy of Classifications of Remotely
582 Sensed Data. Remote Sensing of Environment 46, 35–46.

583 Coops, N.C., Johnson, M., Wulder, M. A., White, J.C., 2006. Assessment of QuickBird high
584 spatial resolution imagery to detect red attack damage due to mountain pine beetle
585 infestation. Remote Sensing of Environment 103, 67–80.

586 Corbin, J.D., Thomsen, M. A, Dawson, T.E., D'Antonio, C.M., 2005. Summer water use by
587 California coastal prairie grasses: fog, drought, and community composition. Oecologia
588 145, 511–21.

589 Cregg, B.M. 1994. Carbon allocation, gas exchange, and needle morphology of *Pinus ponderosa*
590 genotypes known to differ in growth and survival under imposed drought. Tree Physiology
591 14, 883-898.

592 Dawson, T.E., 1996. Determining water use by trees and forests from isotopic, energy balance
593 and transpiration analyses: the roles of tree size and hydraulic lift. Tree Physiology 16: 263-
594 272.

595 Dawson, T.E., 1998. Fog in the California redwood forest: ecosystem inputs and use by plants.
596 Oecologia 117, 476–485.

597 Dennison, P.E., Brunelle, A.R., Carter, V. A., 2010. Assessing canopy mortality during a
598 mountain pine beetle outbreak using GeoEye-1 high spatial resolution satellite data. Remote
599 Sensing of Environment 114, 2431–2435.

600 del-Val, E., Armesto, J. J., Barbosa, O., Christie, D. A., Gutiérrez, A. G., Jones, C. G., Marquet,
601 P.A., Weathers, K. C., 2006. Rain forest islands in the Chilean semiarid region: fog-
602 dependency, ecosystem persistence and tree regeneration. Ecosystems 9, 598-608.

603 Donovan, L.A., Ehleringer, J.R., 1994. Water stress and use of summer precipitation in a Great
604 Basin shrub community. Functional Ecology 8, 289–297.

605 Dubayah, R.C., 1994. Modeling a Solar Radiation Topoclimatology for the Rio Grande River
606 Basin. Journal of Vegetation Science 5, 627–640.

607 Edburg, S.L., Hicke, J.A., Brooks, P.D., Pendall, E.G., Ewers, B.E., Norton, U., Gochis, D.,
608 Gutmann, E.D., Meddens, A.J., 2012. Cascading impacts of bark beetle-caused tree
609 mortality on coupled biogeophysical and biogeochemical processes. Frontiers in Ecology
610 and the Environment 10, 416–424.

611 Ewing, H. A., Weathers, K. C., Templer, P. H., Dawson, T. E., Firestone, M. K., Elliott, A. M.,
612 & Boukili, V. K. (2009). Fog water and ecosystem function: heterogeneity in a California
613 redwood forest. Ecosystems 12, 417-433.

614 Fischer, D.T., 2007. Ecological and biogeographic impacts of fog and stratus clouds on coastal
615 vegetation, Santa Cruz Island, CA (Doctoral disserations). University of California, Santa
616 Barbara, CA.

617 Fischer, D.T., Still, C.J., Williams, A.P., 2009. Significance of summer fog and overcast for
618 drought stress and ecological functioning of coastal California endemic plant species.
619 Journal of Biogeography 36, 783–799.

620 Floyd, M. L., Clifford, M., Cobb, N. S., Hanna, D., Delph, R., Ford, P., & Turner, D., 2009.
621 Relationship of stand characteristics to drought-induced mortality in three Southwestern
622 pinon-juniper woodlands. Ecological Applications 19, 1223-1230.

623 Fraser, R. H., Latifovic, R., 2005. Mapping insect-induced tree defoliation and mortality using
624 coarse spatial resolution satellite imagery. International Journal of Remote Sensing 26, 193-
625 200.

626 Gessler, P.E., Chadwick, O.A., Chamran, F., Althouse, L., Holmes, K., 2000. Modeling Soil –
627 Landscape and Ecosystem Properties Using Terrain Attributes. Soil Science Society of
628 America 64, 2046–2056.

629 Gitlin, A.R., Sthultz, C.M., Bowker, M.A., Stumpf, S., Paxton, K.L., Kennedy, K., Muñoz, A.,
630 Bailey, J.K., Whitham, T.G., 2006. Mortality gradients within and among dominant plant
631 populations as barometers of ecosystem change during extreme drought. Conservation
632 Biology 20, 1477–86.

633 Guo, Q., Kelly, M., Gong, P., Liu, D., 2007. An Object-Based Classification Approach in
634 Mapping Tree Mortality Using High Spatial Resolution Imagery. GIScience & Remote
635 Sensing 44, 24–47.

636 Gutierrez, A. G., Barbosa, O., Christie, D. A., del-Val, E. K., Ewing, H. A., Jones, C. G.,
637 Marquet, P.A., Weathers, K.C., Armesto, J. J., 2008. Regeneration patterns and persistence
638 of the fog-dependent Fray Jorge forest in semiarid Chile during the past two centuries.
639 Global Change Biology 14, 161-176.

640 Hanson, P.J., Weltzin, J.F., 2000. Drought disturbance from climate change: response of United
641 States forests. The Science of the Total Environment 262, 205–20.

642 Harr, R.D., 1982. Fog drip in the Bull Run municipal watershed, Oregon. Water Resources
643 Bulletin 18, 785-789.

644 Hetrick, W.A., Rich, M, P., Barnes, F.J., Weiss, S.B., 1993. GIS-based Solar Radiation Flux
645 Models. American Society of Photogrammetry and Remote Sensing Technical Papers 3,
646 132–143.

647 Hicke, J. A., Johnson, M.C., Hayes, J.L., Preisler, H.K., 2012. Effects of bark beetle-caused tree
648 mortality on wildfire. Forest Ecology and Management 271, 81–90.

649 Hicke, J. A., Logan, J., 2009. Mapping whitebark pine mortality caused by a mountain pine
650 beetle outbreak with high spatial resolution satellite imagery. International Journal of
651 Remote Sensing 30, 4427–4441.

652 Huang, C.-Y., Anderegg, W.R.L., 2012. Large drought-induced aboveground live biomass losses
653 in southern Rocky Mountain aspen forests. Global Change Biology 18, 1016–1027.

654 Hutley, L. B., Doley, D., Yates, D. J., and A. Boonsaner, 1997. Water balance of an Australian
655 subtropical rainforest at altitude: the ecological and physiological significance of
656 intercepted cloud and fog. Australian Journal of Botany 45, 311-329.

657 Ingraham, N., Matthews, R., 1995. The importance of fog-drip water to vegetation: Point Reyes
658 Peninsula, California. Journal of Hydrology 164, 269–285.

659 Iacobellis, S. F., Cayan, D.R., 2013. The variability of California summertime marine stratus:
660 Impacts on surface air temperatures. Journal of Geophysical Research: Atmospheres 118, 1-
661 18.

662 Johnstone, J. A., Dawson, T.E., 2010. Climatic context and ecological implications of summer
663 fog decline in the coast redwood region. Proceedings of the National Academy of Sciences
664 107, 4533-4538.

665 Junak, S., Ayers, T., Scott, R., Wilken, D., Young, D.A., 1995. A flora of Santa Cruz Island.
666 Santa Barbara, Calif.: Santa Barbara Botanical Garden.

667 Kelly, A.E., Goulden, M.L., 2008. Rapid shifts in plant distribution with recent climate change.
668 Proceedings of the National Academy of Sciences 105, 11823–6.

669 Koepke, D.F., Kolb, T.E., Adams, H.D., 2010. Variation in woody plant mortality and dieback
670 from severe drought among soils, plant groups, and species within a northern Arizona
671 ecotone. Oecologia 163, 1079–90.

672 Lanner, R.L., 1999. Conifers of California. Los Olivos, CA*: Cachuma Press*.

673 Limm, E. B., Simonin, K. A., Bothman, A. G., & Dawson, T. E. (2009). Foliar water uptake: a
674 common water acquisition strategy for plants of the redwood forest. *Oecologia*, *161*(3),
675 449-459.

676 Limm, E. B., & Dawson, T. E. (2010). Polystichum munitum (Dryopteridaceae) varies
677 geographically in its capacity to absorb fog water by foliar uptake within the redwood forest
678 ecosystem. *American Journal of Botany*, *97*(7), 1121-1128.

679 McDowell, N., Pockman, W.T., Allen, C.D., Breshears, D.D., Cobb, N., Kolb, T., Plaut, J.,
680 Sperry, J., West, A., Williams, D.G., Yepez, E.A., 2008. Mechanisms of plant survival and
681 mortality during drought: why do some plants survive while others succumb to drought?
682 New Phytologist 178, 719-733.

683 Macomber, S.A., Woodcock, C.E., 1994. Mapping and Monitoring Conifer Mortality Using
684 Remote Sensing in the Lake Tahoe Basin. Remote Sensing of Environment 266, 255–266.

685 Maggi, K., Meentemeyer, R.K., 2002. Landscape dynamics of the spread of sudden oak death.
686 *Photogrammetric Engineering & Remote Sensing* 68, 1001-1009.

687 Meigs, G.W., Kennedy, R.E., Cohen, W.B., 2011. A Landsat time series approach to characterize
688 bark beetle and defoliator impacts on tree mortality and surface fuels in conifer forests.
689 Remote Sensing of Environment 115, 3707–3718.

690 Meentemeyer, R. K., Rank, N. E., Shoemaker, D. A., Oneal, C. B., Wickland, A. C., Frangioso,
691 K. M., Rizzo, D. M., 2008. Impact of sudden oak death on tree mortality in the Big Sur
692 ecoregion of California. Biological Invasions 10, 1243-1255.

693 Michaelsen, J., Schimel, D.S., Friedl, M.A., Davis, F.W., Dubayah, Ralph, C., 1994. Regression
694 Tree Analysis of satellite and terrain data to guide vegetation sampling and surveys. Journal
695 of Vegetation Science 5, 673–686.

696 Monger, H., Bestelmeyer, B., 2006. The soil-geomorphic template and biotic change in arid and
697 semi-arid ecosystems. Journal of Arid Environments 65, 207–218.

698 Moore, D.M., Lees, B.G., Davey, S.M., 1991. A New Method for Predicting Vegetation
699 Distributions using Decision Tree Analysis in a Geographic Information System.
700 Environmental Management 15, 59–71.

701 Ogle, K., Whitham, T.G., Cobb, N.S., 2000. Tree-Ring Variation in Pinyon Predicts Likelihood
702 of Death following Severe Drought. Ecology 81, 3237–3243.

703 Pederson, B.S. 1998. The role of stress in the mortality of Midwestern oaks as indicated by
704 growth prior to death. Ecology 79, 79-93.

705 Perroy, R.L., Bookhagen, B., Asner, G.A., Chadwick, O.A., 2010. Comparison of gully erosion
706 estimates using airborne and ground-based LiDAR on Santa Cruz Island, California.
707 Geomorphology 118, 288-300.

708 Perroy, R.L., Bookhagen, B., Chadwick, O.A., Howarth, J.T., 2012. Holocene and Anthropocene
709 Landscape Change: Arroyo formation on Santa Cruz Island, California. Annals of the
710 Association of American Geographers 102, 1229-1250.

711 Peterson, S. H., Franklin, J., Roberts, D. A., van Wagtendonk, J. W., (2012). Mapping fuels in
712 Yosemite National Park. Canadian Journal of Forest Research 43, 7-17.

713 Ponette-Gonzalez, A.G., Weathers, K. C., Curran, L. M., 2010. Water inputs across a tropical
714 montane landscape in Veracruz, Mexico: synergistic effects of land cover, rain and fog
715 seasonality, and interannual precipitation variability. Global Change Biology 16, 946-963.

716 Raven, P.H., Axelrod, D.I., 1978. Origin and relationships of the California flora. University of
717 California Press: Berkeley, CA.

718 Sørensen, R., Zinko, U., Seibert, J., 2006. On the calculation of the topographic wetness index:
719 evaluation of different methods based on field observations. Hydrology and Earth System
720 Sciences 10, 101–112.

721 Stone, C., Penman, T., Turner, R., 2012. Managing drought-induced mortality in *Pinus radiata*
722 plantations under climate change conditions: A local approach using digital camera data.
723 Forest Ecology and Management 265, 94-101.

724 Suarez, M.L., Ghermandi, L, Kitzberger, T. 2004. Factors predisposing episodic drought-induced
725 mortality in *Nothofagus*- site, climatic sensitivity and growth trends. Journal of Ecology 92,
726 954-966.

727 Uehara, Y., Kume, A., 2012. Canopy Rainfall Interception and Fog Capture by Pinus pumila
728 Regal at Mt. Tateyama in the Northern Japan Alps, Japan. Arctic, Antarctic, and Alpine
729 Research 44, 143-150.

730 van Mantgem, P.J., Stephenson, N.L., Byrne, J.C., Daniels, L.D., Franklin, J.F., Fulé, P.Z.,
731 Harmon, M.E., Larson, A.J., Smith, J.M., Taylor, A.H., Veblen, T.T., 2009. Widespread
732 increase of tree mortality rates in the western United States. Science 323, 521–524.

733 Vogelmann, H.W.,1973. Fog precipitation in the cloud forests of eastern Mexico. Bioscience
734 23(2), 96-100.

735 Walter, H.S., Taha, L.A. 2000. Regeneration of Bishop pine (*Pinus muricata*) in the absence and
736 presence of fire: a case study from Santa Cruz Island, California. In: Browne, D.R.,
737 Mitchell, K.L, Chaney, H.W., Eds. Proceedings of the fifth California Islands symposium,
738 1999 March 29 to April 1; Santa Barbara, California. San Diego, CA: U.S. Department of
739 the Interior, Mineral Management Service (OCS Study MMS 99-0038): 172-181.

740 Weathers, K. C., Lovett, G. M., Likens, G. E., 1995. Cloud deposition to a spruce forest edge.
741 Atmospheric Environment 29, 665-672.

742 Williams, A P., Still, C.J., Fischer, D.T., Leavitt, S.W., 2008. The influence of summertime fog
743 and overcast clouds on the growth of a coastal Californian pine: a tree-ring study. Oecologia
744 156, 601–11.

745 Williams, A P., 2009. Teasing foggy memories out of Pines on the California Channel Islands
746 using tree-ring width and Stable Isotope approaches (Doctoral disserations). University of
747 California, Santa Barbara, CA.

748 Williams, A., P., Allen, C.D., Millar, C.I., Swetnam, T.W., Michaelsen, J., Still, C.J., Leavitt,
749 S.W., 2010. Forest responses to increasing aridity and warmth in the southwestern United
750 States. Proceedings of the National Academy of Sciences 107, 21289–21294.

751 Wulder, M. A., Dymond, C.C., White, J.C., Leckie, D.G., Carroll, A.L., 2006. Surveying
752 mountain pine beetle damage of forests: A review of remote sensing opportunities. Forest
753 Ecology and Management 221, 27–41.

754 Wycoff, P.H., Clark, J.S. 2002. The relationship between growth and mortality for seven co-
755 occurring tree species in the southern Appalachian Mountains. Journal of Ecology 90, 604-
756 615.

757

758

Figure1

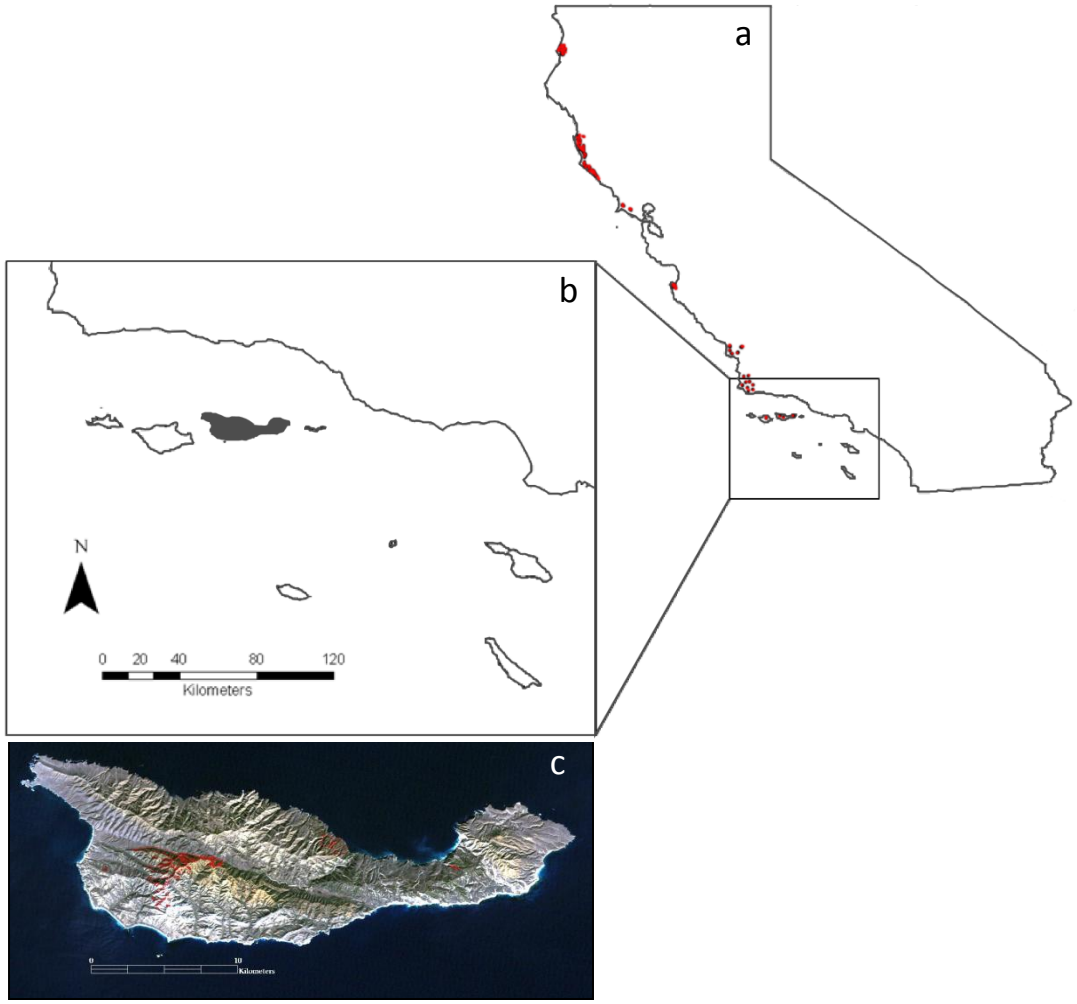

Figure 1. (a) Study area is located on Santa Cruz Island (SCI, 34° N, 119° 45′ W), about 40 km off the coast of Santa Barbara in south-central California, and it supports the southernmost extent of Bishop pine trees in the United States. Other populations in California indicated by red marks along the coastline (Lanner, 1999); (b) SCI (shaded in gray) is the largest of the islands in Channel Islands National Park; (c) Bishop pine stands on SCI are delineated with a red outline. Our study area is the westernmost and largest stand of trees.

Figure2

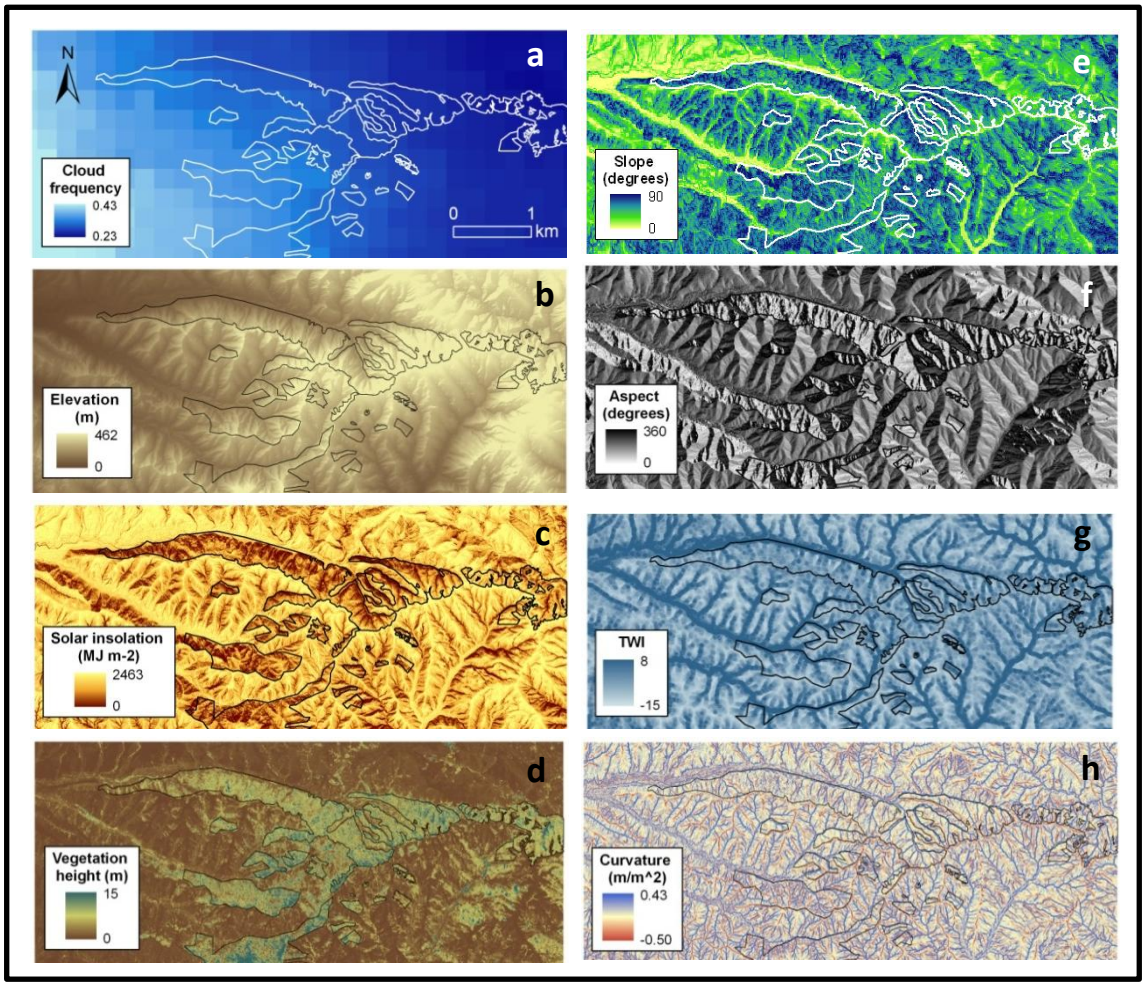

Figure 2. Environmental layers used in the Random Forest analyses. The Bishop pine stand perimeter is delineated in each layer with a white or black line. Layers include: a) summertime cloud frequency, b) elevation (m), c) solar insolation (MJ m^{-2}), d) vegetation height (m), e) slope (degrees), f) aspect (degrees), g) topographic wetness index (TWI), and h) curvature (m m^{-2}).

Figure3

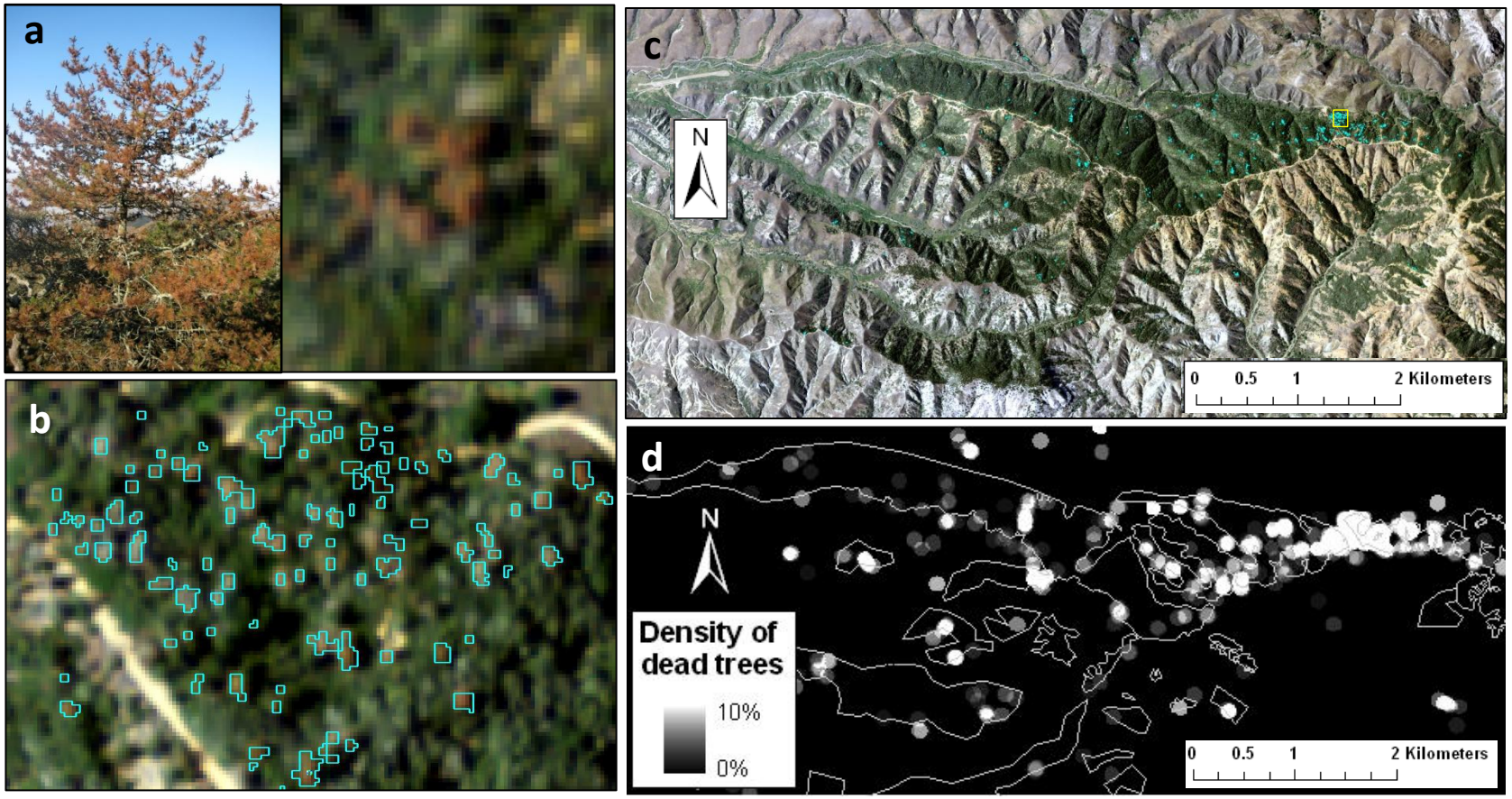

Figure 3. (a) Photograph of a single dead Bishop pine in the field and associated red tree canopies observed in the 2009 true color aerial photo (Digital Ortho Quarter Quad from the U.S.G.S); (b) zoomed in an area highlighted by yellow box in (c) of high tree mortality in the 2009 DOQQ showing individual dead canopies delineated by cyan colored polygons; (c) showing the entire extent of westernmost Bishop pine stand where dead tree canopies (n=871) are indicated by cyan polygons; (d) density map of dead tree canopies where white circles represent average number of dead tree canopy pixels within a 30 m radius of each dead tree. There are only circles where there is a value for tree density. Higher densities of dead trees are represented by the brighter circles. The highest density of dead tree pixels is 10%, which represents about 5-10 dead tree canopies depending on the canopy size. Stand boundaries are given by the polygons (white lines).

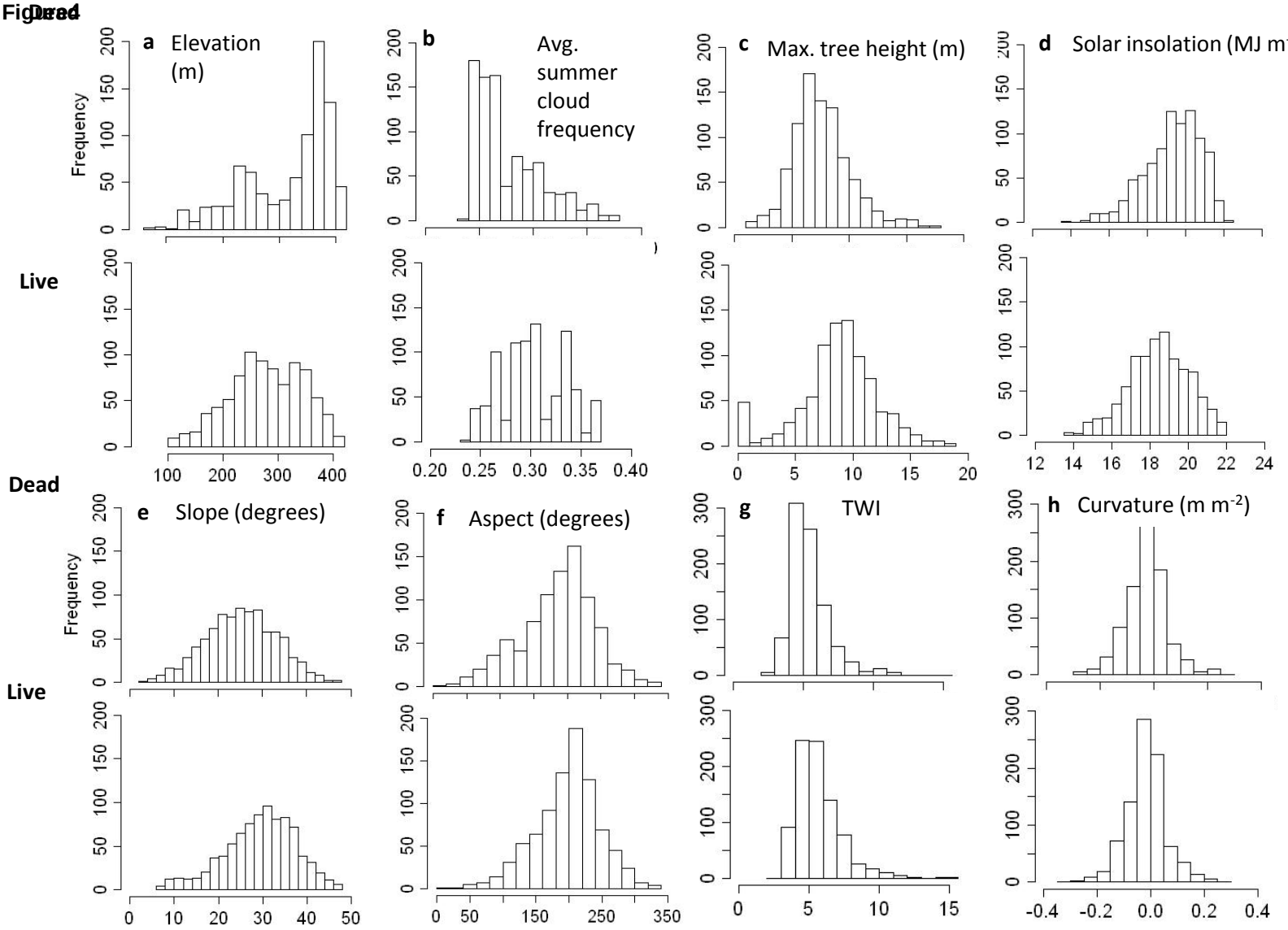

Figure 4. Histogram of variables for dead (above dashed line) and live (below dashed line) tree populations. Differences between median values for live and dead tree populations differed significantly at the $p<0.01$ level, and values are reported in text. To interpret aspect, north-facing =180°, south-facing=360°, west-facing= 90°, and east-facing =270°.

Figure5

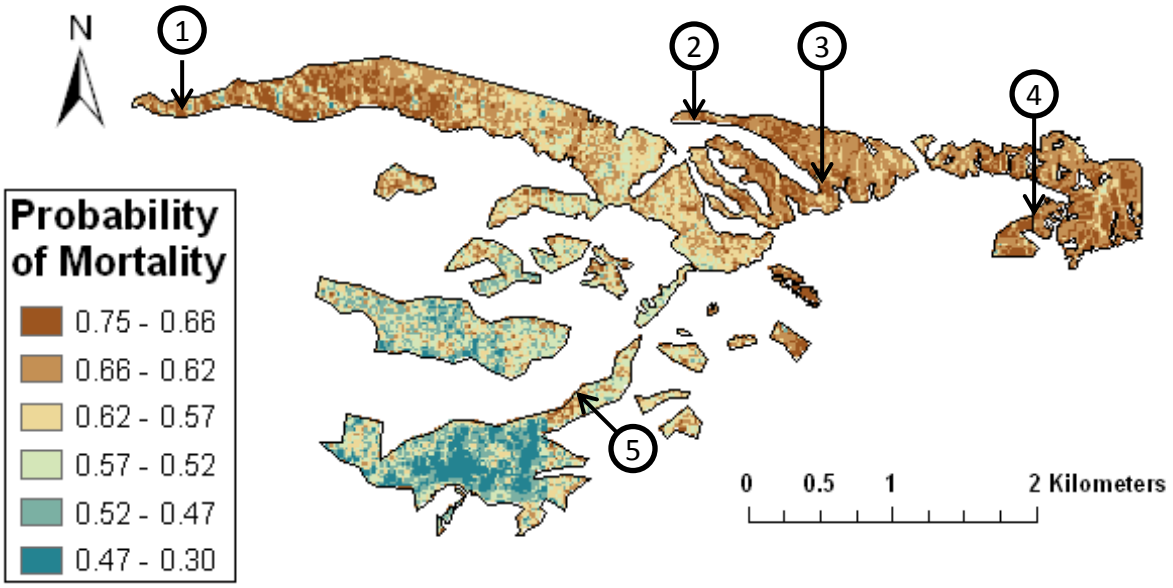

Figure 5. Predictive map of tree mortality following drought for our study area (see Figure 1c for reference). Bishop pine stand is delineated with a black line, and other land surface types are masked out. Red-colored areas represent areas where probability of mortality following drought is high (closer to one) compared to blue-colored areas (closer to 0). Numbered areas (1-5) are described in the text with respect to how probability of mortality relates to environmental conditions and tree height, and are included in Table 5.

Table 1. Potential explanatory variables used in the Random Forest analyses. The Mean Decrease in Accuracy (MDA) value ranks the variables based on how well they separate live and dead tree populations in the RF analysis. The larger the MDA value, the higher ranked the variable, i.e., the greater explanatory power.

Type	Variable	abbreviation	Data source	Spatial scale	Units	MDA
Climatic	Summertime (June-Sept.) cloud cover frequency	clouds	MODIS	250 m	percent	0.84
Topographic	Elevation	elevation	LiDAR DEM	1 m	m	0.79
	Daily integrated summertime (June-Sept.) solar insolation	solar insolation			MJ m^{-2}	0.72
	Slope	slope			degrees	0.70
	Aspect	aspect			degrees	0.63
Geomorphic	Topographic Wetness Index	twi			--	0.36
	Topographic Curvature	curvature			m/m^{-2}	0.28
Biotic	Vegetation Height	veg. height			m	0.81

Table2

Table 2. Average accuracy assessment of 500 decision classification trees in Random Forest analysis.

		Reference			
		Dead	**Live**	**Total**	**User's**
Modeled	**Dead**	674	189	863	0.78
	Live	197	680	877	0.78
	Total	871	869	1740	
	Producer's	0.77	0.78		
	Overall accuracy	0.78			
	Kappa	0.55			

Table3

Table 3. Average probability of tree mortality and environmental variables for the ten sites indicated in Figure 8. Sample locations were determined based on field sites for which we had data on fog-water inputs. The area of each site was approximately 20 m^2.

Site	Probability of mortality (%)	Avg. summer fog-drip (ml)*	Cloud cover frequency	Elevation (m)	Vegetation height (m)	Solar insolation (MJ m^{-2})	Aspect** (degrees)	Slope (degrees)	Curvature (m m^{-2})	TWI
1	70	597	0.32	141	5.4	17.8	208	32	0.041	8.1
2	56	938	0.28	201	9.7	17.6	186	31	-0.033	8.7
3	63	1300	0.26	423	7.8	18.9	115	30	0.076	9.2
4	64	1889	0.24	390	6.0	18.0	176	34	0.128	9.1
5	54	3205	0.31	275	11.1	18.3	131	33	-0.021	7.9

*Fog-drip (ml) data was collected in the field at weather stations (Fischer *et al.*, 2007) from May-September in 2004. We calculated average volume of fog-water inputs over these summer months.
**Aspect: north-facing =180°, south-facing=360°, west-facing= 90°, and east-facing =270°.